Journal of Magnetic Resonance **148,** 23–30 (2001)
doi:10.1006/jmre.2000.2218, available online at http://www.idealibrary.com on IDEAL®

Solution Structure Calculations through Self-Orientation in a Magnetic Field of a Cerium(III) Substituted Calcium-Binding Protein

Ivano Bertini,*,† Matthias B. L. Janik,*,† Gaohua Liu,*,† Claudio Luchinat,†,‡ and Antonio Rosato*,†

*Department of Chemistry, University of Florence, Via Gino Capponi 9, 50121 Florence, Italy; †Centro di Risonanze Magnetiche, University of Florence, Via Luigi Sacconi 6, 50019 Sesto Fiorentino, Italy; and ‡Department of Agricultural Biotechnology, P.le delle Cascine 24, 50100 Florence, Italy

Received March 6, 2000; revised September 6, 2000

Within the frame of a research aimed at characterizing paramagnetic metal ions capable of inducing self-orientation of metalloproteins in solution, we have studied the complex of the 75-amino-acid calcium-binding protein calbindin D_{9k} with one Ce(III) ion (CaCeCb). Backbone ^{15}N–^{1}H ^{1}J values have been determined for CaCeCb at two different magnetic fields. The above values showed a distinct dependence on the magnetic field, which is caused by the partial orientation of the molecule in solution. The difference in the values at the two magnetic fields provides structural constraints, which have been used to refine the structure of CaCeCb. The refined structure showed an improvement in terms of the number of residues falling in favored regions of the Ramachandran plot. The comparison of the molecular magnetic susceptibility tensor, obtained from the ^{15}N–^{1}H ^{1}J values, with the magnetic susceptibility tensor of the metal, obtained from pseudocontact shifts, showed that the orientation of the molecule in solution is mainly determined by the Ce(III) ion. This paper shows that Ce(III), like low-spin Fe(III) in hemoproteins, is sufficiently magnetically anisotropic to induce self-orientation to an extent which can be exploited for solution structure determination.

Key Words: **partial orientation; paramagnetism; magnetic susceptibility; lanthanides; solution structure.**

INTRODUCTION

It has been known for more than 20 years that high magnetic fields may induce partial orientation of molecules experiencing significant magnetic susceptibility anisotropy, yielding effects which are observable by high-resolution NMR (*1–8*). As a consequence, any dipolar coupling does not average zero and the observable is called residual dipolar coupling (rdc).[1] Typically, ^{15}N–^{1}H dipolar couplings, which would average zero in the absence of partial orientation, can be measured (*9*). This effect can be exploited for solution structure determination, since the knowledge of the orientation of, e.g., the NH vectors, helps determine the backbone structure. These constraints are conceptually straightforward and can also be used to determine the quality of a structure through a disagreement factor between calculated and observed ^{1}J values (*10*). The first use of these observables to characterize the molecular orientation tensor of a protein was reported by Bax and colleagues on ubiquitin (*11*). These early studies were followed by structure determinations of DNA–protein complexes (*12*). In order to induce large orientation effects, strategies have been suggested which use orienting aggregates like discotic nematic liquid crystals (also called bicelles) (*13*), membrane fragments (*14*), or viruses (*15*). Depending on the orienting agent used, these may yield an axially symmetric or rhombic orientation tensor.

Our laboratory had explored the possibilities of using magnetically anisotropic metal ions as orienting devices, following the earlier suggestion by Prestegard and co-workers (*9*). Oxidized cytochrome b_5 has a molecular $\Delta\chi_{ax}$ of 2.20×10^{-32} and $\Delta\chi_{rh}$ of -1.34×10^{-32} m^3, and measurable residual dipolar couplings could be obtained, which were used for solution structure refinement (*16*). Owing to the rhombic properties of the magnetic tensor, a rhombic orientation tensor had to be assumed for the solution structure determination (*16*). This implied introducing a rhombic term in the dynamic frequency shift (DFS) correction, as described by Tjandra *et al.* (*11*).

This treatment allowed us to determine the anisotropy of the molecular magnetic tensor, whereas the pseudocontact shift provided the metal magnetic anisotropy. The diamagnetic molecular anisotropy was determined through measurements on the reduced cytochrome, and it was proven that the molecular magnetic susceptibility is the sum of the paramagnetic and the diamagnetic contributions (*16*). Similar studies are available for other cytochromes (*17–19*).

Here we want to explore the possibility of using the lanthanide ion Ce(III). For this purpose the calcium-binding protein calbindin D_{9k} (Ca_2Cb) was used. The protein binds two calcium ions but permits the selective substitution of only one calcium with a lanthanide ion (CaCeCb) (*20*, *21*). Lanthanides are known to provide large magnetic susceptibility anisotropy because of the large spin-orbit coupling constant and the large orbital magnetic moment of *f* orbitals (*22*). Among the lan-

[1] Abbreviations used: Ca_2Cb, calcium-loaded form of calbindin D_{9k}; CaCeCb, complex of calbindin D_{9k} with a single Ce^{3+} ion and a Ca^{2+} ion; NMR, nuclear magnetic resonance; HSQC, heteronuclear single-quantum coherence; pcs, pseudocontact shift; rdc, residual dipolar coupling; DFS, dynamic frequency shift.

1090-7807/01 $35.00

thanides with a paramagnetic ground state, Ce(III) has the most favorable ratio between orienting capability and paramagnetic line broadening and can be conveniently used for the present purpose.

MATERIALS AND METHODS

Sample Preparation

Protein expression (*23*) and purification (*24*) of both the Ca^{2+} and the apo form of bovine calbindin D_{9k} was performed as reported. The Pro43 → Met43 (P43M) mutant representing the minor A form was prepared to avoid any conformational heterogeneity due to *cis–trans* isomerization as found for the wild type (*23, 25*). The expression system was a generous gift of Prof. S. Forsén. Uniformly ^{15}N-labeled P43M was obtained from M9 minimal medium containing $^{15}NH_4Cl$ as the sole nitrogen source. NMR samples were prepared by dissolving the lyophilized protein in 550 μl of either 99% D_2O or 90% H_2O/10% D_2O to finally obtain 2.0 mM protein solutions. The Ca^{2+} form of calbindin D_{9k} was prepared by adding $CaCl_2$ to the apo protein solution in a 2:1 molar ratio. The pH was adjusted to 6.0 by means of 0.1 M NaOH or 0.1 M HCl.

Ce(III) containing P43M calbindin D_{9k} (CaCeCb) samples were obtained by titrating the Ca^{2+} form with 0.1 M solutions of analytical grade $CeCl_3$ (prepared by dissolving Ce_2O_3 (Fluka) in concentrated HCl). Titrations for the ^{15}N-labeled samples were followed by 2D ^1H ^{15}N HSQC spectroscopy. The samples were kept at 4°C in between measurements.

NMR Spectroscopy

NMR spectra for both the CaCeCb and the Ca_2Cb sample were acquired at 300 K on Bruker AVANCE 800 and DRX 500 spectrometers operating at 800.13 and 500.13 MHz, respectively. A series of 15 $^1J_{NH}$-modulated HSQC spectra (*11*) with dephasing delays 2Δ of 44.0, 46.2, 47.4, 48.0, 48.6, 49.8, 51.6, 53.4, 55.2, 57.0, 58.2, 58.8, 59.4, 60.6, and 62.4 ms were recorded. One-bond ^{15}N–^1H coupling constants were subsequently determined by fitting the cross peak intensities to Eq. [1] (*11*),

$$I(2\Delta) = A\cos(2\pi J_{NH}\Delta)\exp(-(2\Delta/T_2^*)), \qquad [1]$$

where $1/T_2^*$ is the effective decay rate of ^{15}N magnetization due to transverse relaxation and unresolved long-range ^{15}N–^1H couplings. A is the intensity of the cross peak for $2\Delta = 0$.

Spectral widths of 14 and 32 ppm in the ^1H and ^{15}N dimension, respectively, were used. The measurements for CaCeCb at 500 MHz were repeated twice to obtain an estimate of the random error. For all experiments, 256 increments with 1024 complex data points each and 32 transients were collected. Raw data were multiplied by a squared cosine window function and Fourier transformed to obtain a final matrix of 1024 × 1024 real data points. A polynominal baseline correction was applied in the f_2 dimension. Resonance intensities were integrated using the Bruker standard software. Rectangular boxes at the noise level were used to define the integration region, except for overlapping cross-peaks, for which smaller boxes were chosen to minimize the contribution from the unwanted peak. A fraction of $2/\pi$ of the duration of the 180° ^{15}N pulse was added to the dephasing delay 2Δ prior to calculating $^1J_{NH}$ to account for the much shorter pulse duration of the 180° ^1H pulse (*11, 26*).

Determination of rdc Values from $^1J_{NH}$ Splittings

The rdc contribution to the $^1J_{NH}$ splitting can be expressed by Eq. [2] (*7*),

$$\mathrm{rdc}(\theta, \phi) = -\frac{1}{4\pi}\frac{B_0^2}{15kT}\frac{\gamma_H\gamma_N h}{4\pi^2 r_{HN}^3}\left[\Delta\chi_{ax}^{mol}(3\cos^2\theta - 1) + \frac{3}{2}\Delta\chi_{rh}^{mol}(\sin^2\theta\cos 2\phi)\right], \qquad [2]$$

where $\Delta\chi_{ax}^{mol}$ and $\Delta\chi_{rh}^{mol}$ are the axial and rhombic components of the molecular susceptibility tensor, χ^{mol}, and θ and ϕ are the cylindric coordinates describing the orientation of the N–H bond vector within the principal axis system of the χ^{mol} tensor. r_{HN} is the length of the N–H bond. All other symbols have their usual meaning. The total $^1J_{NH}$ splitting at a given field is the sum of different individual components (*11*),

$$^1J_{NH}(B_0) = {}^1J_{NH}(0) + \mathrm{rdc}(\theta, \phi) + \delta_{DFS}(B_0), \qquad [3]$$

where $^1J_{NH}(0)$ is the true $^1J_{NH}$ scalar coupling, $\mathrm{rdc}(\theta, \phi)$ is the contribution from the dipolar coupling, and $\delta_{DFS}(B_0)$ is the dynamic frequency shift, which is due to cross correlation between the ^{15}N CSA and ^{15}N–^1H dipolar coupling relaxation mechanisms (*27, 28*). While the rdc and δ_{DFS} values are field dependent, the $^1J_{NH}(0)$ term is removed by measuring the J splittings at two different magnetic fields (18.7 and 11.7 T in the present work) and taking their difference. The difference in rdc values at the two fields (Δrdc) can then be expressed by

$$\Delta\mathrm{rdc}(\theta, \phi) = -[(J_{800\,MHz} - J_{500\,MHz}) + (\delta_{DFS,800\,MHz} - \delta_{DFS,500\,MHz})]. \qquad [4]$$

The negative sign in Eq. [4] takes into account that the $^1J_{NH}$ scalar coupling is negative (*9*), while it is customary to report experimental $^1J_{NH}$ values with positive sign. Equation [2] still holds for the Δrdc values, provided that B_0^2 is replaced by ΔB_0^2.

The δ_{DFS} at a given field depends on the correlation time τ_c and the diffusion properties of the molecule. The principal components of the inertia tensor of Ca_2Cb are 1:0.8:0.8, as calculated from the X-ray structure (*29*), suggesting an isotropic or at least axially symmetric rotational diffusion behavior

in solution. Available ^{15}N relaxation data were used to test whether the rotational diffusion of the protein in solution was best approximated by an anisotropic, axial, or isotropic rotational diffusion model (*30*). The axial model was found to best fit the experimental data. The $D_{\parallel}/D_{\perp}$ ratio was calculated to be 1.2 and the τ_c value to be 4.2 ns. In the axial case the δ_{DFS} values depend on the relative orientation of the principal axes of the diffusion and CSA tensors and on the orientation of the NH bond vector with respect to the two tensors (*11, 31*). The δ_{DFS} value for each ^{15}N nucleus is given by

$$\delta_{DFS}^{CSA-Dipole} = \frac{S^2}{40\pi^3}\, h(\sigma_{\parallel} - \sigma_{\perp})\, \frac{\gamma_N \gamma_H}{r_{NH}^3} \times \left\{ \frac{(3\cos^2\eta_D - 1)(3\cos^2\eta_C - 1)}{1 + (\gamma_N B_0 \tau_1)^{-2}} + \frac{12\cos\eta_D \cos\eta_C \sin\eta_D \sin\eta_C \cos(\phi_D - \phi_C)}{1 + (\gamma_N B_0 \tau_2)^{-2}} + \frac{3\sin^2\eta_D \sin^2\eta_C \cos(2\phi_D - 2\phi_C)}{1 + (\gamma_N B_0 \tau_3)^{-2}} \right\}, \quad [5]$$

where $\tau_1 = (6D_{\perp})^{-1}$, $\tau_2 = (D_{\parallel} + 5D_{\perp})^{-1}$, $\tau_3 = (4D_{\parallel} + 2D_{\perp})^{-1}$. The angle between the NH bond vector and the unique axis of the diffusion tensor is η_D, and that between the axially symmetric CSA tensor and the diffusion tensor, is η_C. The difference $\phi_D - \phi_C$ refers to the angle between projections of the unique axes of the dipolar and CSA tensors on the plane perpendicular to the unique axis of the diffusion tensor; h is Planck's constant, γ_N and γ_H are the gyromagnetic ratios for ^{15}N and ^{1}H, r_{NH} is the N–H internuclear distance (1.02 Å), B_0 is the external magnetic field, and S^2 is the generalized order parameter. An angle of 24° between the ^{1}H–^{15}N vector and the principal axis of the ^{15}N CSA tensor was assumed and a difference between parallel and orthogonal chemical shift for the CSA tensor of ^{15}N of −160 ppm was used (*32*). Residue-specific S^2 values were taken from the literature (*30*). The average contribution from Eq. [5] was found to be 0.09 Hz (from 0.03 to 0.12 Hz).

Determination of the Molecular and Metal Magnetic Susceptibility Anisotropy

The parameters for the molecular susceptibility tensor, χ^{mol}, are obtained by fitting the Δrdc values to Eq. [2]. As the initial input structural model, a family of 30 superimposed conformers calculated without Δrdc constraints was used. The adjustable parameters are $\Delta\chi_{ax}^{mol}$, $\Delta\chi_{rh}^{mol}$, and the three independent direction cosines needed to define the orientation of the tensor within the laboratory frame. The minimized quantity is the sum of the square of the differences between the calculated and experimental Δrdc values. A tolerance of 0.10 Hz was applied.

Analogously, the parameters for the metal susceptibility tensor, χ^{para}, are obtained by fitting the available pseudocontact shift (pcs) values to the following Equation (*33*)

$$\delta^{pcs} = \frac{1}{12\pi r_i^3}\left[\Delta\chi_{ax}^{para}(3\cos^2\theta - 1) + \frac{3}{2}\Delta\chi_{rh}^{para}(\sin^2\theta\cos 2\phi) \right], \quad [6]$$

where $\Delta\chi_{ax}$ and $\Delta\chi_{rh}$ are the axial and the rhombic anisotropies of the magnetic susceptibility tensor, r_i is the distance of the nucleus i from the metal ion, and θ and ϕ are the cylindric coordinates describing the position vector of atom i with respect to the orthogonal reference system formed by the principal axes of the magnetic susceptibility tensor. Again, a family of superimposed conformers calculated without pcs was used as the input structural model. Analogous to the case of Δrdc, the adjustable parameters are $\Delta\chi_{ax}^{para}$, $\Delta\chi_{rh}^{para}$, and the three independent direction cosines needed to define the orientation of the χ^{para} tensor within the laboratory frame. The minimized quantity is the sum of the square of the differences between the calculated and experimental pcs values. Tolerances were set as previously described (*34*).

With the above procedures, average χ^{mol} and χ^{para} tensor parameters for the whole family are determined (*35, 36*). The $\Delta\chi_{ax}$ and $\Delta\chi_{rh}$ values obtained are then used for solution structure calculations together with Δrdc, or Δrdc and pcs constraints, as described in the next section. The resulting family of the best 30 conformers was used as the new input structure for the determination of tensor parameters. The whole procedure was repeated until convergence of the tensor parameters.

Structure Calculations Introducing Δrdc Values

Calculations were performed using the PSEUDYANA (*37*) module of the DYANA program package (*38*) employing torsion angle dynamics combined with a simulated annealing algorithm. Resonance assignments and structural constraints other than Δrdc have been taken from previous work without modifications (*34*). This corresponds to 1539 meaningful NOEs, 6 T_1, and 39 ^{3}J values plus 589 pcs. A new term has been added to the target function of PSEUDYANA in order to incorporate Δrdc constraints, as was previously reported for oxidized cytochrome b_5 (*16*). With the present implementation, in order to use residual dipolar couplings as structural constraints, it is necessary to input to the program Δrdc values and the $\Delta\chi_{ax}^{mol}$ and $\Delta\chi_{rh}^{mol}$ parameters. The relative weights of all constraints were taken equal to 1. A family of 200 conformers was calculated from randomly generated conformers in 10,000 steps of simulated annealing by using all the available constraints, with the exception of pcs constraints larger than 5 ppm in absolute value. The latter pcs were introduced in a subsequent refinement procedure which consisted of a conjugate

gradient minimization with PSEUDYANA using all constraints. The 30 conformers with the lowest target function were subsequently used to recalculate the χ^{mol} and χ^{para} tensor parameters, as mentioned above. These new parameters were used in a new calculation cycle, and the whole procedure was repeated until convergence of the tensor parameters was reached. For comparison, calculations were also performed according to the above procedure, but using only NOE, ^3J, and T_1 constraints plus either Δrdc or pcs constraints.

RESULTS AND DISCUSSION

For the present 75-amino-acid protein a total number of 63 ΔJ values in the case of the Ce^{3+} derivative (CaCeCb) and 69 ΔJ values for the Ca^{2+} form (Ca_2Cb) could be determined. The smaller number of ΔJ values measured for CaCeCb originates from broadening of signals of NH groups close to the paramagnetic center. The ΔJ values roughly cover a range of ± 0.5 Hz and of -1.5 to 0.5 Hz for the diamagnetic (Ca_2Cb) and paramagnetic (CaCeCb) systems, respectively. A list of the values for CaCeCb is given in the supplementary material. A total of 63 Δrdc for CaCeCb and 69 Δrdc for Ca_2Cb were determined from the ΔJ values, as described under Materials and Methods. The largest Δrdc (in absolute value) measured for CaCeCb was 1.26 Hz, which compares to 0.62 Hz for Ca_2Cb. In the case of oxidized cytochrome b_5, the largest Δrdc value was 1.42 Hz (*16*).

Besides those mentioned under Materials and Methods, another phenomenon can contribute to the ^1J splitting, namely the dynamic frequency shift caused by cross-correlation between Curie–dipole and dipole–dipole relaxation (*39*). The latter phenomenon, similar to the dynamic frequency shift caused by cross correlation between CSA and dipole–dipole relaxation and at variance with rdcs, is field independent in the slow motion limit and thus should largely cancel out by taking the difference between the splittings measured at two different fields (as described by Eq. [4]). In the present case, a sizable contribution (of the order of 1.5 Hz) is expected only for one residue (Val 61), whose backbone NH is very close to the metal and favorably oriented. A contribution smaller than 0.2 Hz is expected for all the other residues. However, correction of the Δrdc of Val 61 obtained from Eq. [4] for this effect yields a value which does not fit to either the X-ray or the NMR structure obtained with only NOEs. To better understand this problem, the differences between ^1J splittings recorded at 800 MHz for Ca_2Cb and CaCeCb were inspected. These differences should equal the sum of the *whole* Curie–dipole cross correlation at 800 MHz, plus the difference of Ce and Ca rdcs at the same field. The first contribution is calculated (*39*) to be (in absolute value) as large as 7 Hz for Val 61; in addition residues 24, 51, 54, and 68 should have a contribution (in absolute value) between 0.5 and 1 Hz. The subtraction from the above differences of the Ce rdcs values at 800 MHz (obtained by rescaling the Δrdc values obtained from Eq. [4] by the factor $800^2/(800^2-500^2)$) would yield the pure Curie–dipole cross correlation at 800 MHz, if the Ca rdcs at 800 MHz were negligibly small. Although this is not the case, for the above-mentioned five residues the presence of the Curie–dipole cross correlation effect should be clearly qualitatively observable. Instead, in the present case, there is no evidence for an influence of Curie–dipole cross correlation effects on the measured splittings. Indeed, the differences between the 800-MHz splittings of the CaCeCb and Ca_2Cb systems and the CaCeCb rdc values at the same field agree quite well. The deviations of these two sets of data for the five mentioned residues is comparable with that observed for the other residues of the protein and do not exceed 0.6 Hz. In particular, for residue 61, for which the calculated contribution from Curie–dipole cross correlation to the $^1J_{NH}$ splitting at 800 MHz is 7 Hz, the present analysis is consistent with a contribution of the order of 0.1 Hz. In summary, it appears that the present measurements are not significantly affected by Curie–dipole cross correlation. Nevertheless, to ensure that all possible biases are avoided, the Δrdc value of Val 61, which was the only residue for which a significant such contribution was predicted, was not included in calculations.

The above-mentioned Δrdc values were used to calculate a family of conformers of calbindin D_{9k}, as described under Materials and Methods. Table 1 reports some statistics on the various families of conformers obtained upon inclusion in calculations of different sets of additional constraints, i.e., Δrdc, pcs (taken from our previous work (*34*)), and pcs together with Δrdc. It can be immediately noted that the increase in the target function value upon introduction of the new constraints is quite small. Calculations with pcs constraints display a larger increase of the target function with respect to calculations with Δrdc constraints. This is probably due to the larger number of the former constraints. In all cases the average target function values of the various families of conformers are in the range of those typically reported for good solution structures. The RMSD values of the NOE-only family are essentially the same of those of the family calculated with Δrdc, which instead are somewhat higher than that for the family calculated with pcs. The combined use of pcs and Δrdc constraints does not improve further the precision of the family with respect to calculations with pcs only, but it leads to an improvement in the accuracy, as judged from the *R* factor (*10*) (see below). The behavior of the RMSD values as a function of the various constraints used can be rationalized on the basis of the small number of Δrdc constraints with respect to the number of both NOE and pcs constraints. As expected, the number and magnitude of deviations between experimental pcs and Δrdc values and those calculated from the various families are smaller in the structures obtained using the above data as constraints. This is also evident from Fig. 1, which shows a comparison of calculated and experimental Δrdc values before and after refinement. The plot obtained using the X-ray structure as input model is also reported, showing that the agree-

TABLE 1
Constraints Used for Structure Calculations Together with the Final Target Functions and the Root-Mean-Square Deviations of Atomic Coordinates from the Mean for Ce^{3+} Substituted Calbindin D_{9k}

Additional constraints included in calculations[a]	Average target function[b]	Backbone RMSD[b,c] (Å)	All heavy atoms RMSD[b,c] (Å)	Average deviation of pcs constraints (ppm)	Average deviation of Δrdc constraints (Hz)
—	0.10	0.74 ± 0.13	1.10 ± 0.10	0.5 ± 1.5	0.25 ± 0.20
63 Δrdc	0.53	0.75 ± 0.12	1.13 ± 0.11	0.5 ± 1.5	0.10 ± 0.07
589 pcs	1.15	0.52 ± 0.13	0.97 ± 0.13	0.16 ± 0.48	0.23 ± 0.18
63 Δrdc and 589 pcs	1.81	0.56 ± 0.13	1.01 ± 0.12	0.16 ± 0.47	0.10 ± 0.07

[a] All calculations have been run using 1539 NOEs, 6 T_1, and 39 ^3J-derived constraints in addition to those indicated.
[b] For 30 structures.
[c] Residues 2 to 75.

ment of this structure with the Δrdc values is intermediate between that of the NMR structures obtained with and without Δrdc constraints.

It has been proposed that, by quantifying the agreement between experimental and calculated Δrdc values, it is possible to define an *R* factor for NMR structures in analogy with the *R* factor of crystal structures (*10*). The *R* factor of NMR structures scales between 0 and 1, where a value of 0 indicates perfect agreement between calculated and experimental data, and a random structure yields a value of 1. In the present case, the structure calculated only with NOEs displays an *R* factor of about 0.65. For comparison, the *R* factor calculated on the X-ray structure is roughly 0.5. Refinement yields a dramatic improvement of the *R* factor, in that the refined structure has an *R* value as low as 0.25. The refinement of the structure of the protein cyanovirin-*N* with more than 300 rdc constraints yielded a value for the *R* factor of around 0.16 (*10*), which is similar to that obtained in this work. Finally, the inclusion of Δrdc constraints resulted in an increase of the percentage of residues in the structure belonging to the most favored regions of the Ramachandran plot. The family calculated with pcs only had ca. 77% of the residues in the most favored regions, while this figure increased to 82% upon inclusion of Δrdc constraints. The impact of Δrdc constraints in defining the conformation of the protein backbone, and thus in determining the number of residues falling in favored regions of the Ramachandran plot, had been discussed before (*12*). Remarkably, the family of conformers obtained with NOE data alone had only 72% of the residues in favored regions of the Ramachandran plot, suggesting that the introduction of pcs is also important for properly defining the conformation of the backbone of the protein.

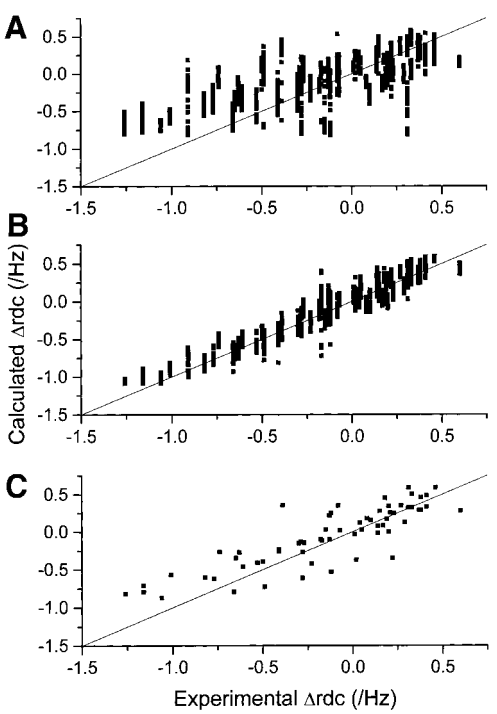

FIG. 1. Comparison of observed versus calculated residual dipolar couplings before (A) and after (B) structure refinement with the Δrdc constraints. Data relative to all the thirty conformers of the family are shown. C reports, for comparison, the same plot using Δrdc values calculated from the X-ray structure. In all panels, to guide the eye, the diagonal is also shown.

The small Δrdc values measured for the diamagnetic Ca_2Cb system were not used to attempt a refinement of the solution structure, due to their relatively large indetermination. Within their indetermination, these values are indeed consistent with both the X-ray and the NMR structure. Nearly all of the Δrdc values measured for Ca_2Cb are negative, indicating that the orientation of the molecule is determined by the helices. This situation is analogous to that of reduced cytochrome b_{562}, a four-helix bundle, whose orientation is largely due to the four parallel long α-helices (*19*).

The Magnetic Susceptibility Tensors

Table 2 reports the parameters describing the magnetic susceptibility tensor of the metal and of the whole molecule calculated after structure refinement with the rdc couplings. From the data in Table 2 it can be observed that the magnitude of the magnetic susceptibility tensor of cerium is similar to that

TABLE 2

Comparison of the Molecular and Metal Magnetic Susceptibility Tensors of Ce^{3+}-Substituted Calbindin D_{9k} Obtained after Calculations with Different Sets of Constraints

	Rdc only[a]	Pcs only[a]	Rdc and pcs
$\Delta\chi_{ax}^{mol}(/10^{-32}m^3)$	1.60 ± 0.08	na	1.75 ± 0.10
$\Delta\chi_{rh}^{mol}(/10^{-32}m^3)$	0.04 ± 0.06	na	0.04 ± 0.07
$\Delta\chi_{ax}^{para}(/10^{-32}m^3)$	na	1.86 ± 0.06	2.03 ± 0.06
$\Delta\chi_{rh}^{para}(/10^{-32}m^3)$	na	0.54 ± 0.05	0.88 ± 0.08

[a] na, not applicable.

of the magnetic susceptibility tensor of the whole molecule. In addition, it is apparent from Fig. 2, which shows the orientation of the χ^{para} and χ^{mol} tensors within the protein frame, that the orientation of the two tensors is also quite similar. There is a relatively large difference in the orientation of the *x* and *y* axes of the two tensors, while the two *z* axes are nearly coincident. However, as the χ^{mol} tensor is essentially axially symmetric (i.e., $\Delta\chi_{rh}$ is nearly zero), the *x* and *y* directions are not well determined.

This difference in the magnitude of the metal and molecular tensors is partly due to the diamagnetic contribution of the molecular magnetic susceptibility of the polypeptide chain. From the small Δrdc values measured in Ca_2Cb it is possible to evaluate the latter contribution. Indeed, the direction with the largest magnetic susceptibility for the diamagnetic molecule lies essentially in the *xy* plane of the magnetic susceptibility tensor of the metal, oriented such as to cancel partially its in-plane anisotropy. On the other hand, the diamagnetic contribution to the $\Delta\chi_{ax}$ component of the molecular tensor is small and cannot account for the observed difference between the latter and the $\Delta\chi_{ax}$ component of the metal tensor. From the present data, it thus appears that $\Delta\chi_{ax}^{mol}$ is about 15% smaller than $\Delta\chi_{ax}^{para}$. The smaller magnitude of the $\Delta\chi_{rh}^{mol}$ component does not allow us to make a reliable estimate of the deviation of the in-plane anisotropy, as it would be somewhat affected by the experimental error. A similar phenomenon had already been reported for the case of the cyanide adduct of myoglobin (*40*), whereas it was not observed in analogous studies on two different *b*-type cytochromes (*16, 19*). The reasons for the difference between $\Delta\chi^{mol}$ and $\Delta\chi^{para}$ in the present system are being investigated.

As mentioned above, the contribution of the diamagnetic part of the molecule (i.e., of the polypeptide chain) to the molecular magnetic susceptibility is relatively small. This is in qualitative agreement with the fact that the absolute values of the Δrdc measured for Ca_2Cb span a range which is approximately a factor of 2 smaller than for CaCeCb. This behavior is largely different from the case of paramagnetic hemoproteins, where the diamagnetic contribution to the molecular magnetic susceptibility, due to the presence of the heme, is always comparable to that of the metal (*9, 16, 40*). Of course, one should keep in mind that particular protein fold topologies might make the contribution of the polypeptide chain to the molecular magnetic susceptibility quite large, e.g., in the case of four-helix bundles (*19*).

CONCLUDING REMARKS

In this work, the solution structure calculation of the paramagnetic complex of calbindin D_{9k} with one Ce(III) and one Ca(II) ion (CaCeCb), using simultaneously Δrdc and pcs constraints, has been reported. As in the case of the paramagnetic oxidized cytochrome b_5, which contains a low-spin Fe(III) ion, there is good consistency between these two sets of nonstandard constraints, as well as with all other classical constraints (NOEs, ^3J values). Both metal ions have only one unpaired electron, and their magnetic anisotropy is of the same order of magnitude. Indeed, the magnetic anisotropy of the Fe(III) ion is somewhat larger (ca. 40%) than that of Ce(III). However, due to the partial cancellation between the "orienting force" of the Fe(III) ion and the heme moiety, the molecular magnetic anisotropy of CaCeCb is only roughly 20–25% smaller than that of oxidized cytochrome b_5.

The present results show that, by exploiting the self-orientation of complexes of proteins with paramagnetic metal ions in the presence of high magnetic fields, it is possible to obtain rdc which are easily and accurately measurable. These can be then used for structure calculation purposes, improving the quality of the structure (e.g., as indicated by the number of residues falling in favorable regions of the Ramachandran plot or by the recently proposed *R* factor (*10*)).

A small, but appreciable, difference (ca. 15%) has been observed between the magnetic susceptibility tensor of the whole molecule and the sum of those of the metal ion and of

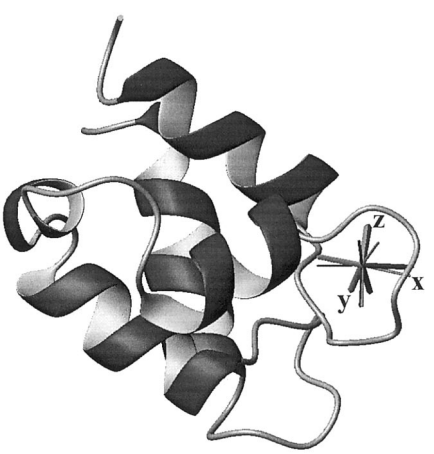

FIG. 2. Display of the orientation of the magnetic susceptibility tensor of the Ce(III) ion (dark gray) and of the whole molecule (light gray) within the molecular frame. The labeling refers to the axes of the magnetic susceptibility tensor of the Ce(III) ion. The *z* axes of the two tensors are nearly coincident. This figure was prepared with the program MOLMOL (*43*).

the polypeptide chain. Other, more paramagnetic, lanthanides can be used instead of cerium to induce a larger orientation of the system in solution (*41*, *42*). The investigation of the occurrence of the discrepancy observed here for cerium in these systems, and of its determinants at the atomic level, will be the subject of further studies.

ACKNOWLEDGMENTS

Thanks are expressed to Prof. Sture Forsén for providing us with the expression system for calbindin D_{9k}. Financial support of the EU through Contract BIO4-98-0156 is gratefully acknowledged. This work has been also partly supported by MURST, ex 40%, and CNR (Contract 99.00393.49).

REFERENCES

1. J. A. B. Lohman and C. Maclean, Magnetic field induced alignment effects in ^{2}H NMR spectra, *Chem. Phys. Lett.* **58,** 483–486 (1978).
2. J. A. B. Lohman and C. Maclean, Alignment effects on high resolution NMR spectra induced by the magnetic field, *Chem. Phys.* **35,** 269–274 (1978).
3. J. A. B. Lohman and C. Maclean, Magnetic susceptibility anisotropies from quadrupolar magnetic field effects in high field ^{2}H NMR, *Mol. Phys.* **38,** 1255–1261 (1979).
4. J. A. B. Lohman and C. Maclean, The determination of magnetic susceptibility anisotropies from quadrupolar interactions in NMR, *J. Magn. Reson.* **42,** 5–13 (1981).
5. J. P. Domaille, Direct measurement of the electron susceptibility anisotropy in paramagnetic complexes using high-field deuterium NMR, *J. Am. Chem. Soc.* **102,** 5392–5393 (1980).
6. A. A. Bothner-By, J. P. Domaille, and C. Gayathri, Ultra high-field NMR spectroscopy: Observation of proton–proton dipolar coupling in paramagnetic bis[tolyltris(pyrazolyl)borato]cobalt(II), *J. Am. Chem. Soc.* **103,** 5602–5603 (1981).
7. P. C. M. van Zijl, B. H. Ruessink, J. Bulthuis, and C. Maclean, NMR of partially aligned liquids: magnetic susceptibility anisotropies and dielectric properties, *Accounts Chem. Res.* **17,** 172–180 (1984).
8. A. A. Bothner-By, C. Gayathri, P. C. M. van Zijl, C. Maclean, J.-J. Lai, and K. M. Smith, High-field orientation effects in the high-resolution proton NMR spectra of diverse porphyrins, *Magn. Reson. Chem.* **23,** 935–938 (1985).
9. J. R. Tolman, J. M. Flanagan, M. A. Kennedy, and J. H. Prestegard, Nuclear magnetic dipole interactions in field-oriented proteins: Information for structure determination in solution, *Proc. Natl. Acad. Sci. USA* **92,** 9279–9283 (1995).
10. G. M. Clore and D. S. Garret, R-factor, free R, and complete cross-validation for dipolar coupling refinement of NMR structures, *J. Am. Chem. Soc.* **121,** 9008–9012 (1999).
11. N. Tjandra, S. Grzesiek, and A. Bax, Magnetic field dependence of nitrogen-proton *J* splittings in ^{15}N-enriched human ubiquitin resulting from relaxation interference and residual dipolar coupling, *J. Am. Chem. Soc.* **118,** 6264–6272 (1996).
12. N. Tjandra, J. G. Omichinski, A. M. Gronenborn, G. M. Clore, and A. Bax, Use of dipolar ^{1}H–^{15}N and ^{1}H–^{13}C couplings in the structure determination of magnetically oriented macromolecules in solution, *Nat. Struct. Biol.* **4,** 732–738 (1997).
13. N. Tjandra and A. Bax, Direct measurement of distances and angles in biomolecules by NMR in a diluite liquid crystalline medium, *Science* **278,** 1111–1114 (1997).
14. J. Sass, F. Cordier, A. Hoffmann, M. Rogowski, A. Cousin, J. G. Omichinski, and S. Grzesiek, Purple membrane induced alignment of biological macromolecules in the magnetic field, *J. Am. Chem. Soc.* **121,** 2047–2055 (1999).
15. G. M. Clore, M. R. Starich, and A. M. Gronenborn, Measurement of residual dipolar couplings of macromolecules aligned in the nematic phase of a colloidal suspension of rod-shaped viruses, *J. Am. Chem. Soc.* **120,** 10571–10572 (1998).
16. L. Banci, I. Bertini, J. G. Huber, C. Luchinat, and A. Rosato, Partial orientation of oxidized and reduced cytochrome b_5 at high magnetic fields: Magnetic susceptibility anisotropy contributions and consequences for protein solution structure determination, *J. Am. Chem. Soc.* **120,** 12903–12909 (1998).
17. H. Déméné, P. Tsan, P. Gans, and D. Marion, NMR determination of the magnetic susceptibility anisotropy of cytochrome *c′* of *Rhodobacter capsulatus* by $^1J_{HN}$ dipolar coupling constants measurement: Characterization of its monomeric state in solution, *J. Phys. Chem. B* **104,** 2559–2569 (2000).
18. J. C. Hus, D. Marion, and M. Blackledge, De novo determination of protein structure by NMR using orientational and long-range order restraints, *J. Mol. Biol.* **298,** 927–936 (2000).
19. F. Arnesano, L. Banci, I. Bertini, Karin van der Wetering, M. Czisch, and R. Kaptein, The auto-orientation in high magnetic field of oxidized cytochrome b_{562} as source of constraints for solution structure determination, *J. Biomol. NMR* **17,** 295–304 (2000).
20. H. J. Vogel, T. Drakenberg, S. Forsén, J. D. O'Neil, and T. Hofmann, Structural differences in the two calcium binding sites of the porcine intestinal calcium binding protein: A multinuclear NMR study, *Biochemistry* **24,** 3870–3876 (1985).
21. M. Akke, S. Forsén, and W. J. Chazin, Molecular basis for cooperativity in Ca^{2+} binding to calbindin D_{9k}. ^{1}H nuclear magnetic resonance studies of (Cd^{2+})1-bovine calbindin D_{9k}, *J. Mol. Biol.* **220,** 173–189 (1991).
22. B. Bleaney, Nuclear magnetic resonance shifts in solution due to lanthanide ions, *J. Magn. Reson.* **8,** 91–100 (1972).
23. P. Brodin, T. Grundstrom, T. Hofmann, T. Drakenberg, E. Thulin, and S. Forsén, Expression of bovine intestinal calcium binding protein from a synthetic gene in *Escherichia coli* and characterization of the product, *Biochemistry* **25,** 5371–5377 (1986).
24. C. Johansson, P. Brodin, T. Grundstrom, E. Thulin, S. Forsén, and T. Drakenberg, Biophysical studies of engineered mutant proteins based on calbindin D9K modified in the pseudo EF-hand, *Eur. J. Biochem.* **187,** 455–460 (1990).
25. A. Malmendal, G. Carlström, C. Hambraeus, T. Drakenberg, S. Forsén, and M. Akke, Sequence and context dependence of EF-hand loop dynamics. An ^{15}N relaxation study of a calcium-binding site mutant of calbindin D_{9k}, *Biochemistry* **37,** 2586–2595 (1998).
26. R. R. Ernst, G. Bodenhausen, and A. Wokaun, "Principles of Nuclear Magnetic Resonance in One and Two Dimensions," Oxford Univ. Press, London, 1987.
27. M. Guéron, J. L. Leroy, and R. H. Griffey, Proton nuclear magnetic relaxation of ^{15}N-labeled nucleic acids via dipolar coupling and chemical shift anisotropy, *J. Am. Chem. Soc.* **105,** 7262–7266 (1983).
28. M. Goldman, Interference effects in the relaxation of a pair of unlike spin-1/2 nuclei, *J. Magn. Reson.* **60,** 437–452 (1984).
29. D. M. E. Szebenyi and K. J. Moffat, The refined structure of vitamin D-dependent calcium-binding protein from bovine intestine. Molecular details, ion binding, and implications for the structure of other calcium-binding proteins, *J. Biol. Chem.* **261,** 8761–8777 (1986).
30. M. Akke, N. J. Skelton, J. Kördel, A. G. Palmer, III, and W. J.

Chazin, Effects of ion binding on the backbone dynamics of calbindin D_{9k} determined by ^{15}N NMR relaxation, *Biochemistry* **32,** 9832–9844 (1993).

31. L. Werbelow, Dynamic frequency shift, *in* "Encyclopedia of Nuclear Magnetic Resonance" (D. M. Grant and R. K. Harris, Eds.) pp. 1776–1783, Wiley, Chichester, 1996.

32. Y. Hiyama, C. H. Niu, J. V. Silverston, A. Bavoso, and D. A. Torchia, Determination of ^{15}N chemical shift tensor via ^{15}N–^{2}H dipolar coupling in Boc-glycylglycyl[^{15}N]glycine benzyl ester, *J. Am. Chem. Soc.* **110,** 2378–2383 (1988).

33. H. M. McConnell and R. E. Robertson, Isotropic nuclear resonance shifts, *J. Chem. Phys.* **29,** 1361–1365 (1958).

34. M. Allegrozzi, I. Bertini, M. B. L. Janik, Y.-M. Lee, G. Liu, and C. Luchinat, Lanthanide induced pseudocontact shifts for solution structure refinements of macromolecules in shells up to 40 A from the metal ion, *J. Am. Chem. Soc.* **122,** 4154–4161 (2000).

35. I. Bertini, C. Luchinat, and A. Rosato, The solution structure of paramagnetic metalloproteins, *Progr. Biophys. Mol. Biol.* **66,** 43–80 (1996).

36. D. Bentrop, I. Bertini, M. A. Cremonini, S. Forsén, C. Luchinat, and A. Malmendal, The solution structure of the paramagnetic complex of the N-terminal domain of calmodulin with two Ce^{3+} ions by ^{1}H NMR, *Biochemistry* **36,** 11605–11618 (1997).

37. L. Banci, I. Bertini, M. A. Cremonini, G. Gori Savellini, C. Luchinat, K. Wüthrich, and P. Güntert, PSEUDODYANA for NMR structure calculation of paramagnetic metalloproteins using torsion angle molecular dynamics, *J. Biomol. NMR* **12,** 553–557 (1998).

38. P. Güntert, C. Mumenthaler, and K. Wüthrich, Torsion angle dynamics for NMR structure calculation with the new program DYANA, *J. Mol. Biol.* **273,** 283–298 (1997).

39. R. Ghose and J. H. Prestegard, Electron spin-nuclear spin cross-correlation effects on multiplet splittings in paramagnetic proteins, *J. Magn. Reson.* **128,** 138–143 (1997).

40. J. R. Tolman, J. M. Flanagan, M. A. Kennedy, and J. H. Prestegard, NMR evidence for slow collective motions in cyanometmyoglobin, *Nat. Struct. Biol.* **4,** 292–297 (1997).

41. M. A. Contreras, J. Ubach, O. Millet, J. Rizo, and M. Pons, Measurement of one bond dipolar couplings through lanthanide-induced orientation of a calcium-binding protein, *J. Am. Chem. Soc.* **121,** 8947–8948 (1999).

42. R. R. Biekofsky, F. W. Muskett, J. M. Schmidt, S. R. Martin, J. P. Browne, P. M. Bayley, and J. Feeney, NMR approaches for monitoring domain orientations in calcium-binding proteins in solution using partial replacement of Ca^{2+} by Tb^{3+}, *FEBS Lett.* **460,** 519–526 (1999).

43. R. Koradi, M. Billeter, and K. Wüthrich, MOLMOL: A program for display and analysis of macromolecular structure, *J. Mol. Graphics* **14,** 51–55 (1996).